Investigation of a new steel-concrete connection for composite bridges

Dimitrios Papastergiou [*1] and Jean-Paul Lebet [2a]

[1] *DIC s.a. ingénieurs, Aigle, Switzerland*
[2] *Steel Structures Laboratory, EPFL École Polytechnique Fédérale de Lausanne, Switzerland*

Abstract. A new type of connection for steel-concrete composite bridges was developed by the Steel Structures Laboratory of Ecole Poytechinque Fédérale de Lausanne. Resistance to longitudinal shear is based on the development of shear stresses in the confined interfaces which form the connection. Confinement is provided by the reinforced concrete slab which encloses the connection and restrains the uplift (lateral separation) of the interfaces by developing normal stresses. The experimental investigation of the interfaces, under static and cyclic loading, enabled the development of the laws describing the structural behaviour of each interface. Those laws were presented by the authors in previous papers. The current paper focuses on the continuity of the research. It presents the experimental investigation on the new connection by means of push-out tests on specimens submitted to static and cyclic shear loading. Investigation revealed that the damage in the connection, due to cyclic loading, is expressed by the accumulation of a residual slip. A safe fatigue failure criterion is proposed for the connection which enabled the verification of the connection for the fatigue limit state with respect to the limit of fatigue. A numerical model is developed which takes into account the laws describing the interface behaviour and the analytical expressions for the confinement effect, the latter obtained by performing finite element analysis. This numerical model predicts the shear resistance of the connection and enables to assess its fatigue limit which is necessary for the fatigue design proposed.

Keywords: steel-concrete connection; interfaces; shear; slip; uplift; confinement; cyclic loading; fatigue damage; composite bridges

1. Introduction

In steel-concrete composite bridge construction with prefabricated slab elements, the traditional solution to apply the composite action between the slab elements and the steel girders is concreting the openings (shear pockets) of the slab elements in which shear studs are enclosed. Studs are typically welded on the upper part of the flanges of the girders. However this method presents several disadvantages. The supplementary work in situ for concreting the pockets increases the overall construction time. Due to the development of shrinkage in the concrete of the shear pockets

---

*Corresponding author, Ph.D., Bridge Engineer, E-mail: dtpapastergiou@gmail.com
[a] Processor, Ph.D., Director of the Steel Structures Laboratory of Ecole Polytechnique Fédéral de Lausanne

and due to stress concentration, cracks appear at the perimeter and at the corner of the shear pockets. Corrosion agents such as de-icing salt which enter the cracks might decrease the durability of the structure and damage the connection. Those disadvantages are overcomed using a new type of connection by adhesion, interlocking and friction (Thomann and Lebet 2007, Papastergiou and Lebet 2011) which are favourable for prefabrication and help guarantee long term durability. The new connection, in comparison with other new innovative solutions, as for example steel dowels created on the steel web by cutting a steel profile (Feldmann *et al.* 2008, Rauscher and Hegger 2008) or connections with perfobond ribs (Kim and Jeong 2010), present the advantage that allow for prefabrication without supplementary cast in place concrete for the deck. Fig. 1 presents the new connection.

The steel girder is provided with a pair of longitudinal connecting plates. Those embossed steel plates are welded together and are also welded longitudinally to the upper flange of the steel girder. The deck consists of precast reinforced concrete segments which are fabricated with a rib at the lower part. The surface of the rib is roughened by using a retarding agent during casting, followed by hydro-jetting and sandblasting. The aggregates on the rib surface are exposed but firmly attached to the concrete mass. The slab segments are positioned over the steel connector and are connected together by prestressing, see Fig. 2. The void between the connector and the concrete deck is filled with a high strength cement grout by injection. Once the cement grout is cured the connection is activated and composite action can be achieved.

The resistance of the connection to longitudinal shear is based on the shear stresses that are developed at two types of interfaces. The two types include an interface between the embossed steel and the cement grout and an interface between cement grout and the concrete deck, as illustrated in Fig. 1. Due the development of the longitudinal shear, τ, in the connection, interfaces tend to slip, see Fig. 3. Due to the roughness of the interface, this slip, s, is accompanied by an uplift (lateral separation) of materials, u, at a direction normal to the slip, s. This lateral separation, u, is however restrained due to the, normal stress, σ, (confinement effect) created by the surround-
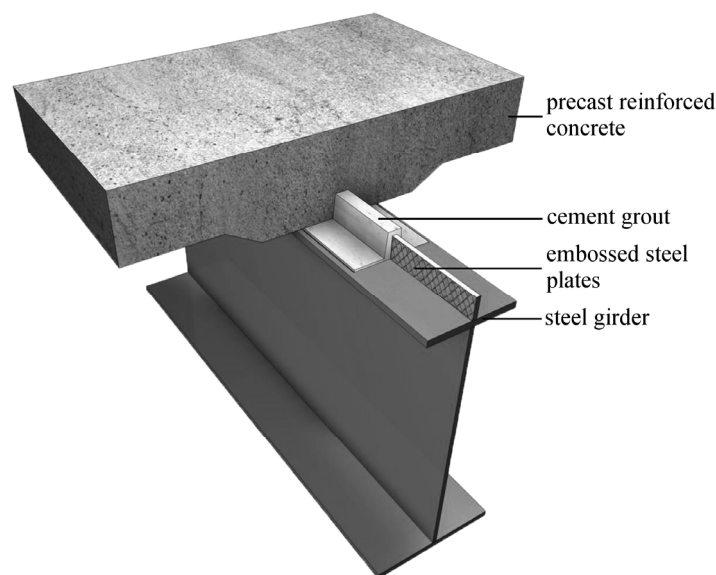

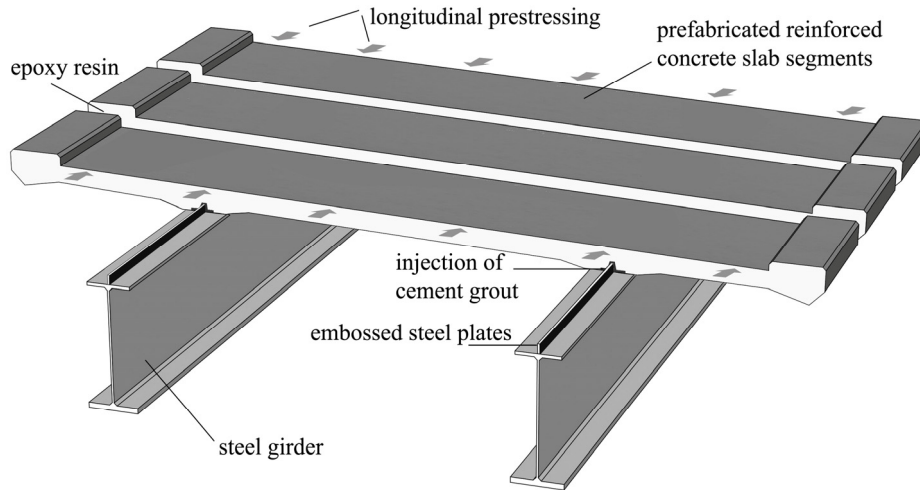Fig. 1 Connection by adhesion, interlocking and friction

Fig. 2 Typical cross section of a highway steel-concrete composite bridge realised with the connection by adhesion, interlocking and friction

ing concrete slab. An equilibrium state is developed with tension in the concrete and in the reinforcement of the concrete slab over the rib and normal compression stresses developed on the interfaces. Fig. 4 illustrates the equilibrium state caused by the uplift (lateral separation) in the embossed steel-cement grout interface. Equally, uplift between the roughened concrete and cement grout is also developed but not presented in this figure. The confinement effect provided by the slab on the interfaces of the connection becomes even more significant if, in addition, the normal forces resulting from the transversal bending of the slab, after the cure of the cement grout of the connection, are considered.

The three laws describing the interfaces behaviour were presented by the authors in previous paper (Papastergiou and Lebet 2011). These laws are: (a) the relationship between the shear failure stress, τ_u, and the normal stress, σ, acting on the interface, called hereafter *failure criterion*; (b) the relationship, under normal constant stress, between the shear stress, τ, and the slip, s, in an interface, called hereafter *constitutive law*; and (c) the relationship, under normal constant stress, between the uplift (lateral separation), u, and the slip, s, in an interface, called hereafter *kinematic law*.

However, the interfaces laws by themselves are not sufficient to describe the connection behaviour. This is due to the fact that in reality the normal stress, σ, developed in the interface,
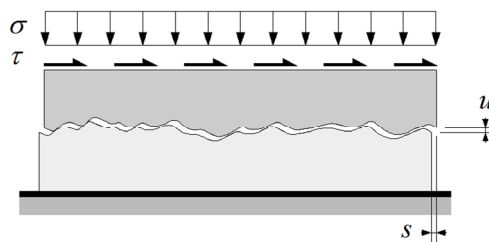

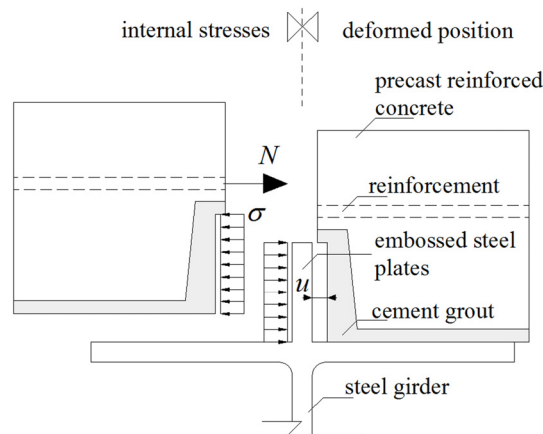Fig. 3 Definition of interface parameters

Fig. 4 Development of confinement due to uplift (lateral separation)

from the confinement imposed by the slab, is not constant but varies. Consequently, in addition to the constitutive law and the kinematic law for constant normal stress the relationship between the normal stress, σ, and the uplift, u, in other words the relationship describing the confinement effect, is needed in order to study the connection behaviour. This relationship is found by performing parametrical finite element analysis on the connection's section using the ABAQUS software (2011). In this analysis the steel rebars are considered as embedded constrains. For the concrete the stress-strain diagram according to FIB (2010) is used for material property. Both uncracked and cracked concrete behaviour are considered. This analysis, presented in detail by the authors in previous work (Papastergiou 2012), enabled to develop analytical expressions for the normal stress-uplift relationship (confinement effect).

In the continuity of the research for the new connection, the current paper presents the experimental investigation of the connection's behaviour for static and cyclic loading by performing push-out tests on specimens fabricated with the new connection. It presents also the numerical model developed to predict the connection behaviour. This model takes into account the mentioned above laws which are describing the interface behaviour, the analytical expressions for the confinement effect and their interaction. The experimental data obtained was used to validate the numerical model and enabled to propose a safe fatigue failure criterion for the new connection. Finally, using the numerical model, the connection's fatigue limit is assessed and is used for the verification of the connection at fatigue limit state.

2. Experimental investigation

2.1 Principles of the test

The connection's behaviour was investigating by performing push-out tests on specimens fabricated with the new connection. Both static and cyclic loading tests were performed. A push-out specimen consists of two blocks of reinforced concrete assembled together with a steel connector by filling the void between them with cement grout. Fig. 5 presents the principle of the push-out test.
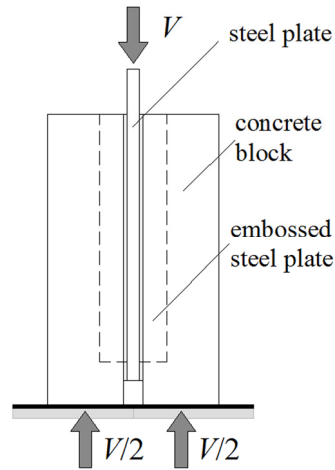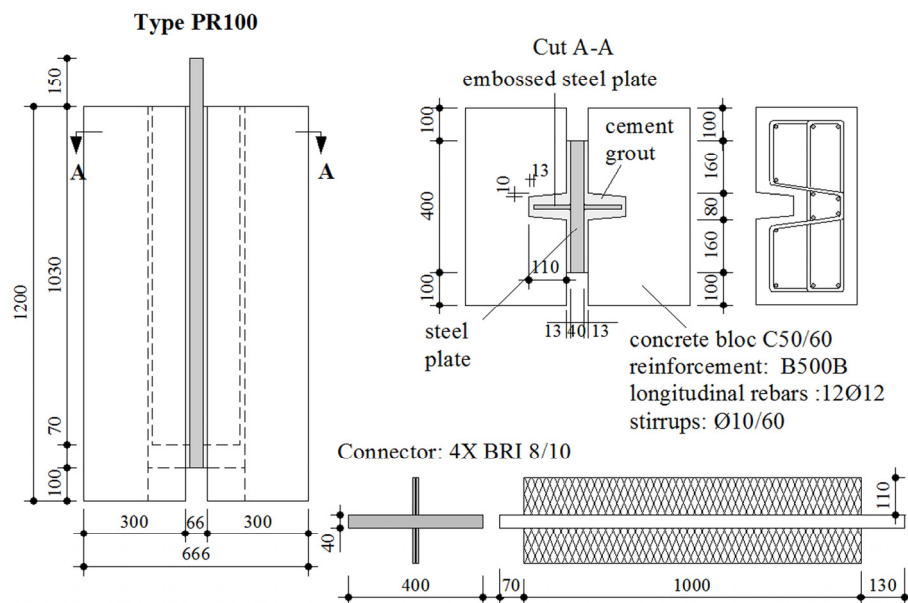
Fig. 5 Principal of the push-out test

Fig. 6 Geometrical characteristics of push-out specimens consisted of blocks of reinforced concrete, steel connector and cement grout

The force, V, is applied to the steel element of the specimen and then is transmitted by shear, through the interfaces, to the blocks of reinforced concrete and from them to the base of the testing setup.

2.2 Specimens and materials

Twelve symmetrical specimens for push-out tests have been fabricated. Fig. 6 illustrates the geometry of the parts which constitute the specimens and the assembly as well. The blocks for the

twelve specimens are made of reinforced concrete-concrete quality C50/60 according to Eurocode 2 (2004). Granularity is of maximum diameter 16 mm. The surface of the concrete plates was roughened by sand-blasting from a distance of 60 cm, with pressure 4.5 bars and for 40 seconds. The formwork used for the surfaces that were sand-blasted was covered with the retarding agent of type Pieri DRC 6/130. A typical roughened surface of a concrete block is illustrated in Fig. 7a. The steel rebars of the concrete blocks are of type B500B and their covering 40 mm. The steel connector consists of a steel plate in which the embossed steel plates are welded as illustrated in Fig. 7(b). Steel plates are of type S235, sand-blasted. The embossed steel-plate conforms to type BRI 8/10 according to the construction table of the Centre Suisse de la Construction Métallique (2005). The ribs had a width of 5 mm and height of 1.4 mm and formed rhombus with 22 mm and 55 mm long diagonals.

Two different types of cement grout were used. For the first ten specimens the cement grout used was the type of grout used previously by Thomann and Lebet (2007) and for which the interface laws were developed by the authors in previous work. It is a cement grout developed by the VSL Company with water to cement varying from 0.29 to 0.32, containing two admixtures a stabiliser and a plasticizer. Its fluidity measured by performing the Marsh cone flow test is generally around 25 sec. However in some cases the grout presented a thixotropic behaviour and could not guarantee the appropriate fluidity in time. Hence for the last two push-out specimens (PR100_11 and PR100_12 according to Table 1) the commercial product cement grout VSL-HPI (2002), with enhanced characteristics was used. This type of cement grout used commonly in prestressed tendons exhibits no segregation, low porosity and contains an expansive agent counterbalancing shrinkage volume loss. Due to the expansive agent, better bonding conditions are expected between the materials that form the interfaces in the connection, resulting to enhanced structural performance, which was verified experimentally as can been seen later on.
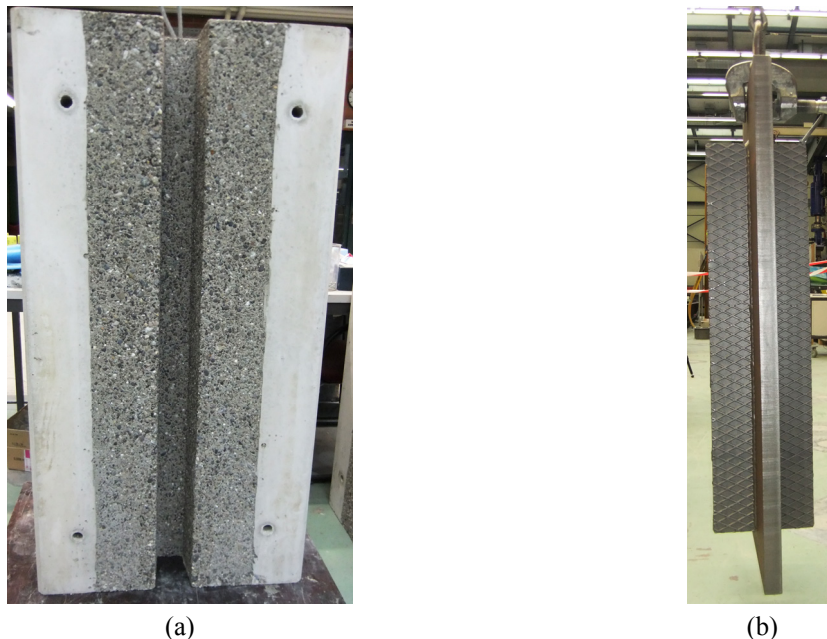

(a)   (b)

Fig. 7 (a) Reinforced concrete block for push-out tests, with rough inner rib and (b) embossed steel plates

Fig. 8 Test set up

(a)

(b)

Fig. 9 Instrumentation at the upper part of the push-out specimen

2.3 Buckling of the axially compressed beam

Tests were performed with the machine Trebel Schenk of the laboratory of the Civil Engineering Institute. The load is applied under displacement control, for static tests, with a loading rate of 0.25 mm/min till failure and 1 mm/min for post-failure loading. Cyclic tests were performed under force control with security limits in the displacement of the hydraulic jack, and with a frequency of 1.5 Hz. During cyclic (pulsar) loading only the shear force is recorded, hence in order to record the evolution of the force-slip relationship, with the number of cycles, the cyclic loading stops at certain moments, and a complete loading-unloading cycle is performed at loading rate 0.25 mm/min to register data. In addition, the unloading allows registering of the residual slip that develops in the connection, with the number of cycles. Fig. 8 illustrates the major instrumentation used for the push-out tests. Eight transducers type HMB (2000), attached at the

steel plate at the first and at the second third of the height of the connector, are used to measure the relative slip between the steel plate and the blocks. At the upper part of the specimen four transducers, two at each connector, serve to measure the uplift (lateral separation) between connector and the concrete blocks, as illustrated in Fig. 9(a). Other transducers are used to measure several displacements between parts of the specimen assembly, as shown in Fig. 9(b).

The fabrication of the twelve push-out specimens took place in a certain period of months to avoid aging of cement sacs for the grout offered by the provider. This fact and the availability of the testing machine had as a result that for several specimens the application of the load was done at a time more than a month from the time of the fabrication of the specimen. For specimens PR100_9 and PR100_10 the produced cement grout lacked fluidity in time and presented a thixotropic behaviour while the removing of formwork has shown lot's of voids on the connection. These voids are verified by diamond cutting of specimens. Hence these two specimens are excluded from the study. These kinds of problems are not however to be encountered in real practice where the cement grout VSL-HPI with enhanced characteristics or other type of cement grout with the adequate fluidity should be used.

Table 1 summarizes the experimental programme and presents the characteristics of the push-out tests. Notation f_{cm} stands for the mean cement grout resistance at 28 days after the fabrication. V_{min} and V_{max} correspond to the lower and higher values of the applied load for cyclic loading, where V_u corresponds to the ultimate load. Notation t_o stands for the time from the specimens' fabrication till the application of the load, whereas t for the time from the specimens' fabrication till the application of the load at the final test that follows the runnout.

Due to the limited number of available specimens the control of the connection shear resistance to fatigue loading was decided to be performed with respect to the limit of fatigue. The cyclic loading values mentioned in Table 1 correspond to the expected values of the longitudinal shear for this type of connection used to form a twin-I type steel girder-concrete deck composite bridge

Table 1 Cyclic shear loading tests for an embossed steel-cement grout interface

Specimen (name)	f_{cm} (N/mm^2)	t_0 (days)	t (days)	V_u (kN)	V_{min} (kN)	V_{max} (kN)	V_{max}/V_u	executed cycles
PR100_1	86.4	50	-	2538	-	-	-	1
PR100_2	86.4	78	127	2565	260	1060	0.41	5E+6
PR100_3	76.4	32	-	1836	-	-	-	1
PR100_4	76.4	33	-	-	260	1060	-	4E+6*
PR100_5	94.3	109	152	2407	260	1060	0.44	5E+6
PR100_6	94.3	107	-	1963	-	-	-	1
PR100_7	99.4	185	230	3081	260	1600	0.52	5E+6
PR100_8	99.4	145	171	2900	260	1600	0.55	2E+6
PR100_9	123.8	32	-	1801	-	-	-	1
PR100_10	123.8	33	-	1795	-	-	-	1
PR100_11	66.8	28	91	4130	260	1860	0.45	2.5E+6
PR100_12	66.8	94	-	3230	0	variable	-	235**

* test stopped due to jack malfunction damaging the specimen
** 5 cycles of variable amplitude and 230 post failure cycles

section, commonly used in Swiss highways, as illustrated in Fig. 2. More precisely the minimum applied load 260 kN corresponds to longitudinal shear per unit length equal to 130 kN/m. This value is a mean value of the longitudinal shear acting in the connection for long term loads such as dead loads from coating, cornice and safety barrier.

Verification of connection with respect to the limit of fatigue according to fatigue load model 1 of the Swiss code SIA 261 (2003), which corresponds to fatigue load model 1 of the Eurocode 1 (2003), Fig. 10(a), implies for the region of end support of a composite bridge an added variation of the longitudinal shear, Δv_D, of 400 kN/m (value corresponding to short end span about 30 m long, longer spans have lower values), thus the total value of longitudinal shear rises up to 530 kN/m. Consequently, this verification imposes a maximum load for the push-out tests, V_{max}, equal to 1060 kN. Verification of the connection with respect to the fatigue limit according to a load
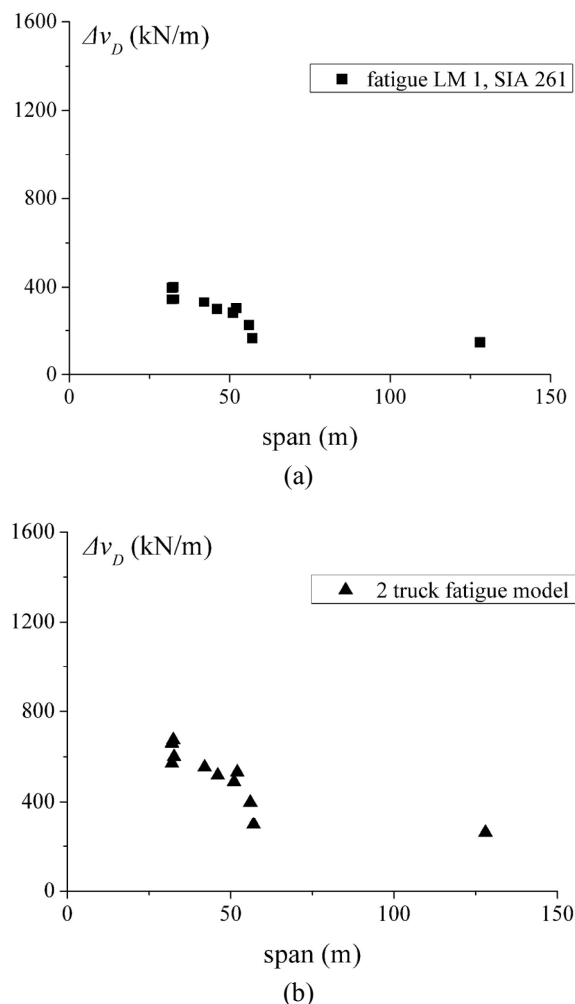

(a)

(b)

Fig. 10 Required resistance to longitudinal shear with respect to the fatigue limit for end support connections using (a) the fatigue load model 1 of code SIA 261; and (b) a deterministic model with 2 trucks, 60 and 45 tons respectively

model based on real traffic data, proposed by Meystre and Lebet (2011), implies for the region of end support of a composite bridge an added variation of the longitudinal shear, Δv_D, of 670 kN/m, Fig. 10(b), (value corresponding to short end span about 30 m long), resulting to a total value for the longitudinal shear of 800 kN/m. Consequently the maximum cyclic load for the push-out tests, V_{max}, for this check, raises up to 1600 kN/m.

For the specimen PR100_11, fabricated with the cement grout with enhanced characteristics, a higher value of V_{max} equal to 1860 kN was chosen due to the higher expected resistance.
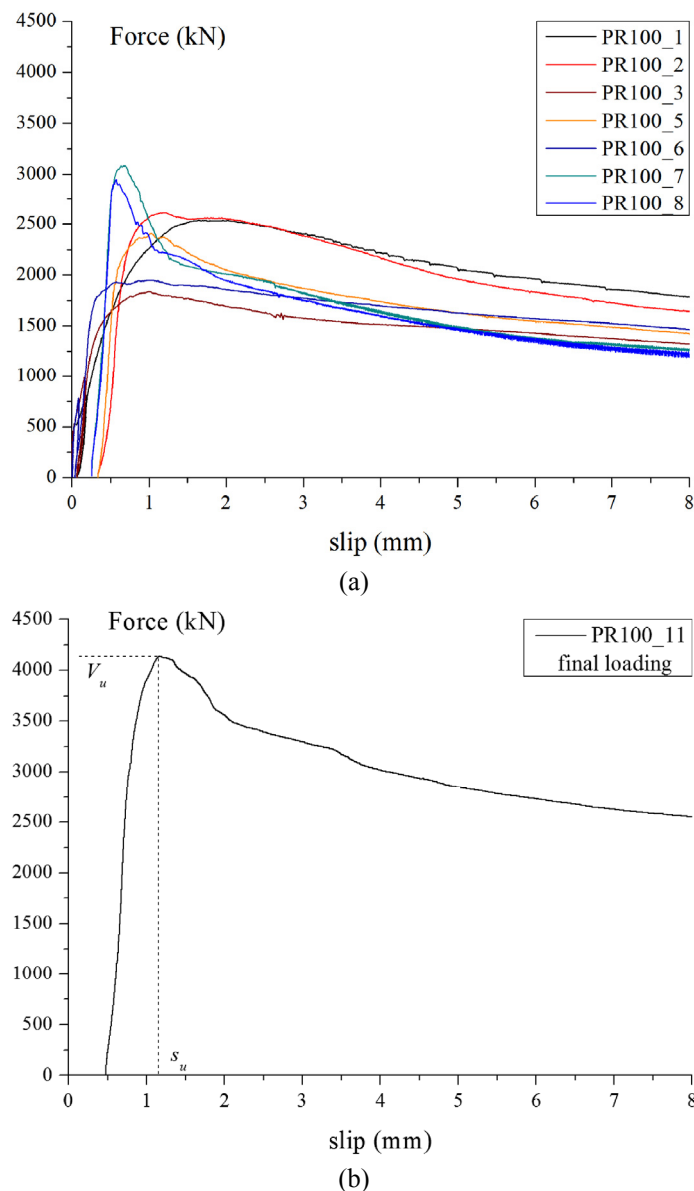

Fig. 11 Force-slip relationship for push-out specimens: (a) with cement grout VSL and (b) with cement grout VSL-HPI

3. Results and discussion

3.1 Static loading

Figs. 11(a)-(b) illustrate the force-slip relationship (slip is the average of the values measured with the transducers) obtained from static loading, including static tests which follow runout cyclic loading tests. Hence, for the latter, the initial slip is different from zero and corresponds to the residual slip which develops during the cyclic loading. According to Fig. 11(a) the resistance of the specimens varies. Generally specimens filed with cement grout of the same fabricated mixture develop similar resistance. Diamond cutting of failed specimens permits to do several observations which justify the reduced resistance of specimens PR100_3 and PR100_6, as described later on.

Generally the connection exhibits a primary stiff ascending branch prior to failure, meaning that the longitudinal shear force per unit length increases followed by a moderate slip, between concrete blocks and the steel plate, which at failure point, V_u, varies from 0.7 to 1.8 mm. Once the ultimate resistance is reached, failure initiates expressed by an increase of the slip. The post failure branch is characterised also by a decrease of the resistance, which can be abrupt (specimens PR100_7 and PR100_8) or ductile.

The force-slip relationship for specimen PR100_11 is presented in Fig. 11(b). This specimen is filled with another type of cement grout, the VSL-HPI grout, which despite its reduced compression resistance in comparison with the cement grout of the specimens of Fig. 11(a), contains an expansive agent that promises better bonding conditions between the materials that form the interfaces and consequently better structural performance. Figs. 12(a)-(b) illustrate, for the specimens of Figs. 11(a)-(b) respectively, the uplift-slip relationship. The uplift in this case is the transversal separation between the steel connector and the block, at the upper part of the specimen. This value is the half of the value measured by transducers, see Fig. 9(b), since the transducers measure the uplift (lateral separation) of both sides from the connector. The presented
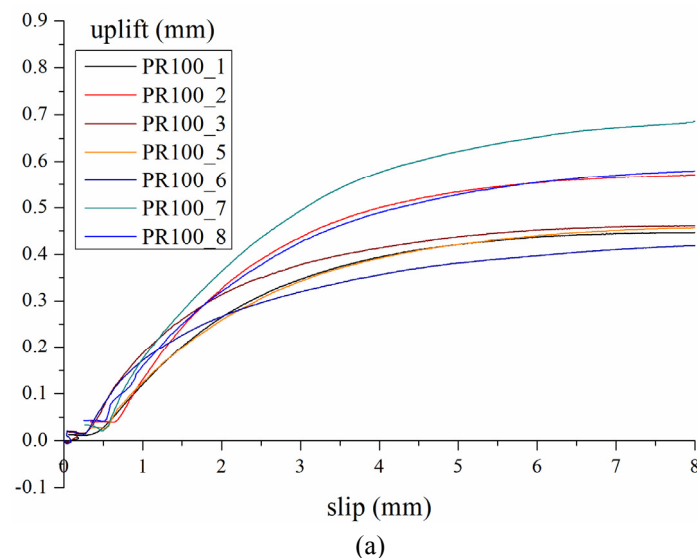

(a)

Fig. 12 Uplift (lateral separation)-slip relationship for push-out specimens: (a) with cement grout VSL; and (b) with cement grout VSL-HPI
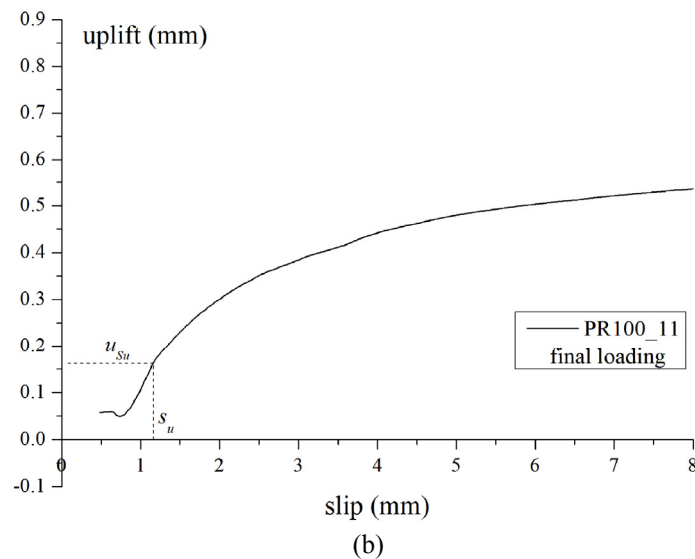
(b)

Fig. 12 Continued

uplift corresponds to the addition of the uplift between rough concrete-cement grout and the uplift of embossed steel plate - cement grout, with the second part being the most significant. Uplift (lateral separation) in the interface presents prior to failure load V_u relatively low values, generally less than 0.2 mm. After failure, i.e., $s > s_u$, uplift increases to an asymptotic value which is achieved at about 8 mm of average slip in the interface.

Fig. 13(a) illustrates a typical example of the development of cracks at the upper part of the concrete blocks of the push-out specimens. Cracks initiate in the cement grout at the end of the connector and propagate inside the reinforced concrete block. Initially cracks are inclined and they are redirected vertically at the level of the position of the lower transverse reinforcement. Cracks close at the level of the upper reinforcement. In some cases some secondary inclined cracks are formed sourcing from the main vertical crack. As noticed in Fig. 13(a), the slip between the concrete block and the connectors corresponds mostly to the relative slip between the embossed plates of the connector and the cement grout. The relative slip between rough concrete and cement grout is hardly noticed. The same conclusion is reached when examining the failure surface as obtained after diamond cutting of failed specimens. Figs. 14 and 15 present the view obtained after cutting the failed specimen PR100_5. The main mass of cement grout is separated from the embossed steel plates. Shear type of failure of cement grout inside the rhombus, is noticed. As illustrated, the failure surface develops between the embossed steel-plate and the cement grout. Any slip between rough concrete and cement grout is relative small since, after the diamond cutting procedure, the cement grout remains attached to the rough concrete (Fig. 15). Diamond cutting of specimens allows also making several hypotheses for the scatter of the ultimate resistance presented in Fig. 11(a). For the specimen PR100_3 the lower resistance is due to the shear failure of one of the concrete blocks which was found to be cracked. Another important parameter is the positioning of the rebars that provide the confinement. It was found, due to diamond cutting, that the positioning of the rebars was not executed with the same accuracy for all specimens resulting in different confinement and thus different ultimate resistance. The lower
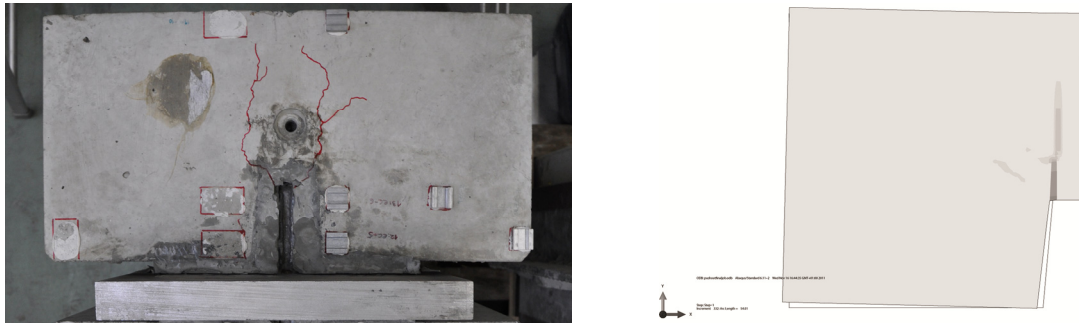
Fig. 13 Cracking of concrete blocks of push-out specimens at the upper part after failure: (a) experimental; (b) from finite element analysis (FEA)
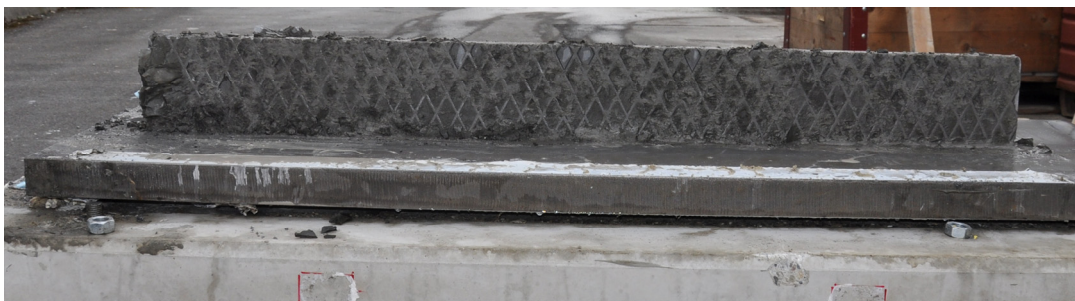

Fig. 14 Steel connector after diamond cutting of block, specimen PR100_5

Fig. 15 Concrete block after diamond cutting. Cement grout remains attached to rough concrete. Specimen PR100_5

resistance of the specimen PR100_6 can be attributed to that reason, as is shown in the Section 4.1. For the specimens PR100_7 and PR100_8 the relatively high ultimate resistance is probably due to aging of the cement grout.

3.2 Cyclic loading

As it is shown in Table 1 six tests of high number constant amplitude cycles and one test with few cycles close to ultimate resistance have been performed. Fig. 16, Figs. 17 and 18 present the
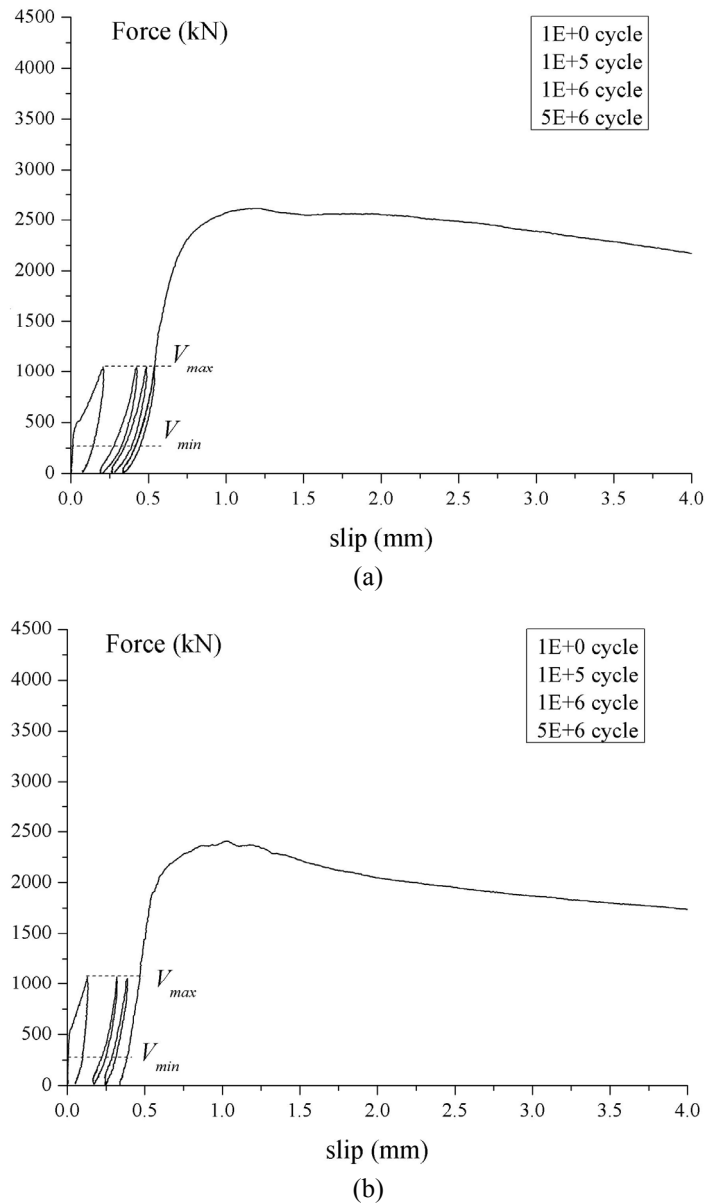
Fig. 16 Force-slip relationship for push-out specimens: (a) PR100_2; and (b) PR100_5

force-slip relationship for cyclic loading with the three different amplitudes that were mentioned above in Section 2.3.

As seen in those figures an unloading takes place in specific cycles in order to record the residual slip, $s_{res,N}$, which is the expression of the damage due to cyclic loading. The graphs include also the final static loading which follows cyclic loading run outs. The residual slip, $s_{res,N}$, and the slip under maximum cyclic shear load, $s_{Vmax,N}$, are increasing with repeated loading, however those increases tend to stabilize. This stabilization is more clearly seen in Figs. 19 and 20. Comparing

the ultimate resistance of those specimens, at the final static loading, with the ones subjected directly to static loading we obtain the result that the cyclic loading, with the selected amplitude, does not influence the specimens remaining resistance. This behaviour of the new connection for cyclic loading, with is characterised of the stabilization of the residual slip, $s_{res,N}$, and of the slip under maximum cycle shear load, $s_{Vmax,N}$, and the conservation of the ultimate resistance, is similar to the behaviour recorded by the authors (2014) for cyclic loading of the types of interfaces which constitute the connection and for which the maximum applied shear stress does not exceed the
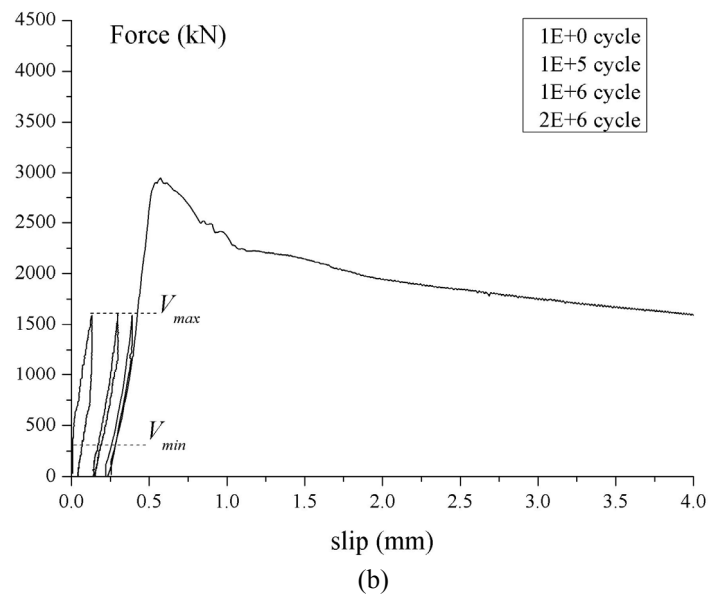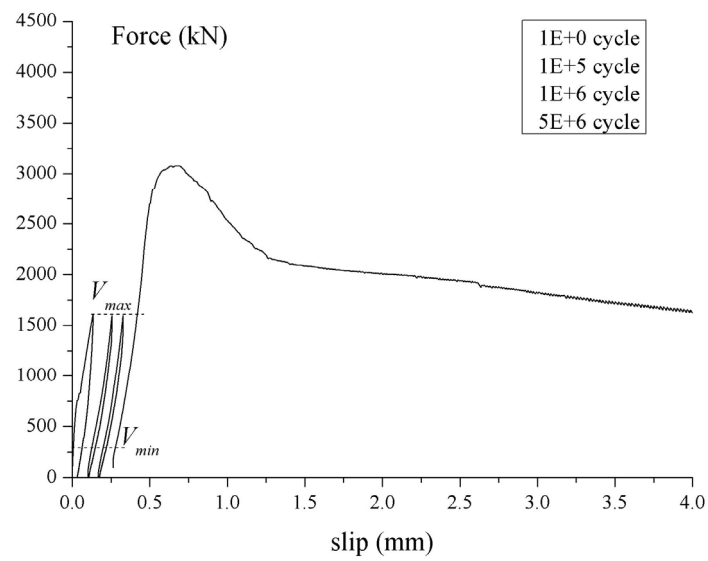

Fig. 17 Force-slip relationship for push-out specimens: (a) PR100_7; and (b) PR100_8
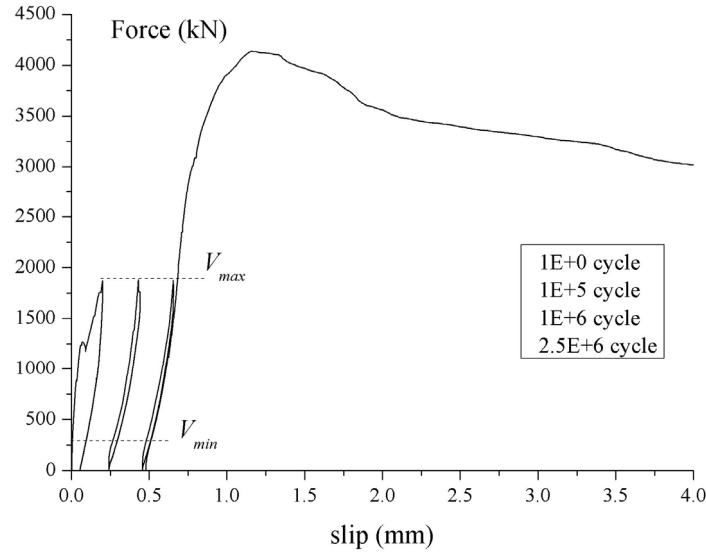
Fig. 18 Force-slip relationship for push-out specimen PR100_11

elastic limit.

A major outcome, from the previous work concerning the cyclic loading of interfaces, was that failure in an interface does not occur, al long as the slip under maximum cyclic shear stress does not exceed the value of the failure slip, s_u, for a virgin static loading. Concerning the connection, where the total slip is the addition of the slip of the two types of interfaces that are formed the same rule applies. In fact we see in Figs. 16 to 18 that the stabilization of the slip at values lower than the value of slip at failure for the final static loading is the reason of the fatigue resistance of the connection. When, however, the slip exceeds the failure slip for static loading, s_u, the connection's resistance to cyclic loading is limited to few cycles, as can been in Fig. 21 for the specimen PR100_12. In this case, failure slip, s_u, was caused by high amplitude cycles close to the ultimate resistance. After failure and for just 230 cycles the shear resistance was limited to the residual shear and the slip increased continuously. From the above and similarly to what was stated for the interfaces, the following safe fatigue failure criterion is proposed for the connection:

No failure due to cyclic loading occurs in the connection as long as the accumulated slip after N cycles under maximum cycle shear load, $s_{V\max,N}$ is inferior to the slip which corresponds to failure for static loading, s_u, Eq.(1).

$$s_{V\max,N} \leq s_u \tag{1}$$

Based on the results on Figs. 19 and 20 analytical expressions are derived from the fitting curves for the residual slip, $s_{res,N}$, and the slip under maximum cyclic shear load, $s_{V\max,N}$, and are presented by Eqs. (2) and (3) respectively.

$$s_{res,N} = s_{res,1} \cdot N^{b_{con,res}} \tag{2}$$

$$s_{V\max,N} = s_{V\max,1} \cdot N^{b_{con}} \tag{3}$$

The equations produced express a power law with parameters the number of cycles, N, the slip
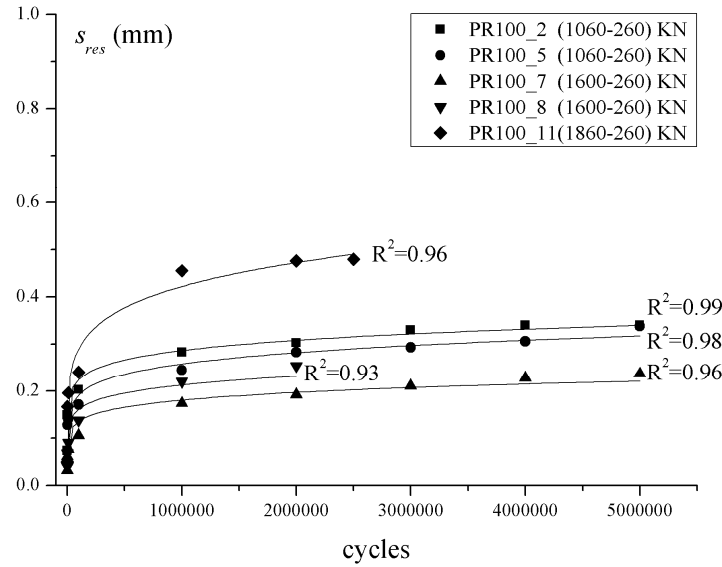
Fig. 19 Residual slip in the connection, s_{res}, after removal of the load, as a function of the number of cycles and fitting curves
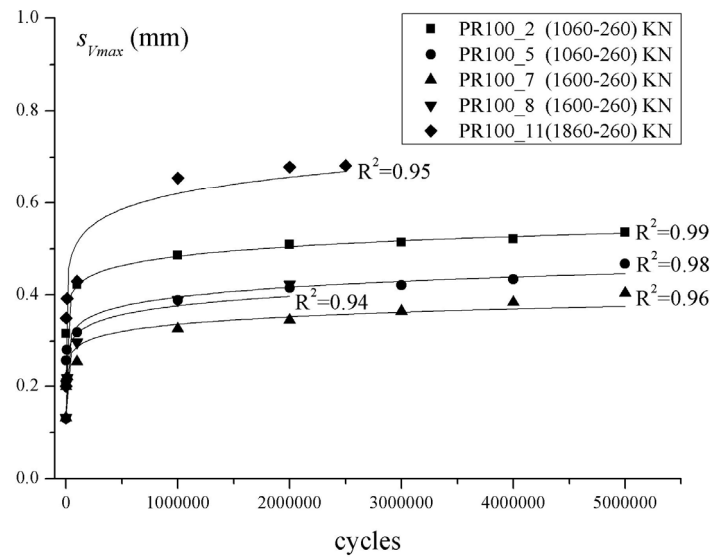

Fig. 20 Slip in the connection under maximum cyclic shear load, s_{Vmax}, as a function of the number of cycles and fitting curves

under maximum cycle shear load and the residual slip, $s_{Vmax,1}$ and $s_{res,1}$, respectively for the first cycle, and the power indexes $b_{con,res}$ and b_{con}; the latter are presented in Table 2 for each test. The mean statistical values for the power indexes $b_{con,res}$ and b_{con} are 0.072 and 0.129 respectively and are close to the value 0.098 proposed by Oh and Kim (2007) for repeated loading of ribbed steel bars embedded in concrete. From substitution in Eq. (1) using Eq. (3) we obtain the number of cycles to failure of the connection, N_f, Eq. (4).

$$N_f = \left(\frac{s_u}{s_{V\max,1}} \right)^{1/b_{con}} \tag{4}$$

In Eq. (4) the slip at failure for static loading, s_u, and the slip for maximum cyclic shear load $V_{\max}$ for the first cycle, $s_{V\max,1}$, are obtained from the force-slip relationship for static loading of push-out specimens fabricated with the new connection. When this is not possible, as it is the common case when designing the connection for a new steel-concrete composite bridge, a scientific tool is needed in order to predict the shear force-slip relationship for static loading. In addition, as it is seen in Table 2 for the specimens tested, the ratio of the maximum applied cycle shear load, $V_{\max}$, versus the ultimate resistance, V_u, for which the stabilization of the residual slip occurs with repeated loading, varies from 0.41 to 0.55. The stabilization of the slip implies, according to previous research of the authors (Papastergiou and Lebet 2014), that the interfaces respond remain elastic. Hence the need raises for a scientific tool which for specific connection geometry will provide a non-arbitrary limit for the limit of the connection's elastic behaviour needed for the verification of the connection with respect to limit of fatigue. These issues are answered in the Section 4 where the numerical model for the connection's behaviour is presented.

Table 2 Recorded power index for the residual slip and slip under maximum cyclic loading

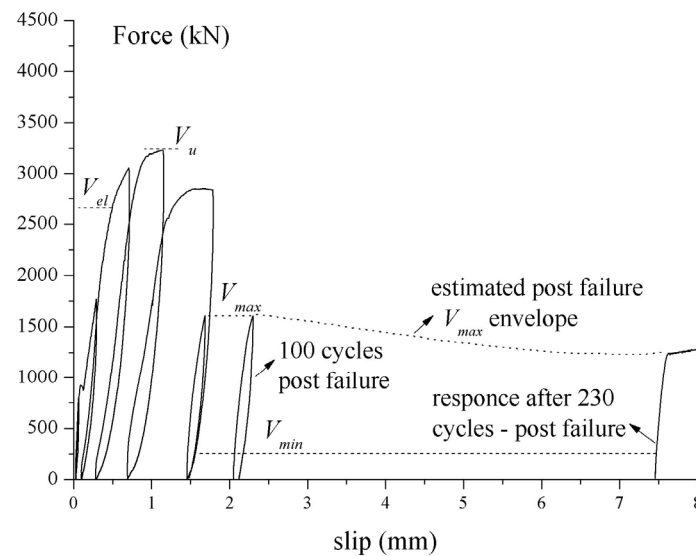| Specimen name	$V_{\max} / V_u$	b_{con}	$b_{con,res}$
PR100_2	0.41	0.062	0.106
PR100_5	0.44	0.075	0.128
PR100_7	0.52	0.068	0.125
PR100_8	0.55	0.076	0.121
PR100_11	0.45	0.082	0.163

Fig. 21 Force-slip relationship for push-out specimen PR100_12

4. Modelling

4.1 Numerical model

The failure criterion, the constitutive law and the kinematic law proposed for the interface behaviour (Papastergiou and Lebet 2011) and (Papastergiou and Lebet 2014) together with the analytical expressions produced for the confinement effect (Papastergiou 2012) and the interaction between them are taken into account in a numerical model. This interaction is schematically described in Fig. 22.

The initial state of an interface in the connection is described by point 1. A pre-existed normal stress σ_1 is acting in the interface prior to loading, due, for example, to the transversal bending of the deck, caused from loads applied after the realisation of the connection and the establishment of the composite action. The uplift (lateral separation), u, and the slip, s, are initially zero. For an incremental slip, Δs, the stress path follows the constitutive law for a normal stress σ_1 and the shear stress reaches the value τ_2. For the same incremental slip the uplift, based on the kinematic law for normal stress σ_1, reaches the value u_2. Due to the relationship between the normal stress and the uplift which is presented in the third (clockwise) quadrant and which describes the confinement effect, the normal stress reaches the value σ_2 (point 2). For further incremental slip Δs, the constitutive and kinematic laws corresponding to normal stress σ_2 are taken into account to define the point 3. The stress path (fourth clockwise quadrant), the evolution of the shear stress with the slip and the actual kinematics of the interface are presented by the dotted lines in Fig. 22. When the stress path intercepts the failure criterion the interface fails. It is noted that in such a model the incremental slip must be limited so that the increase of the normal stress, σ, is gradual. This is required because the coordinates of the point at a specific step are corresponding to the actual normal stress of that step whereas for the same uplift (lateral separation) the normal stress at the confinement relationship is higher (it is the normal stress that defines the next step). In the opposite case iteration should be applied to overcome the mismatch.

Besides the mentioned interaction and the interface laws the numerical model assumes a
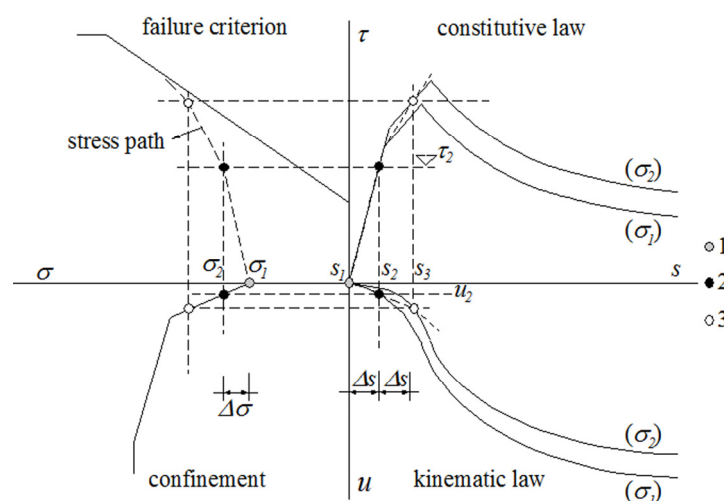

Fig. 22 Schematic presentation of the interaction of the failure criteria, the interface laws and the confinement effect
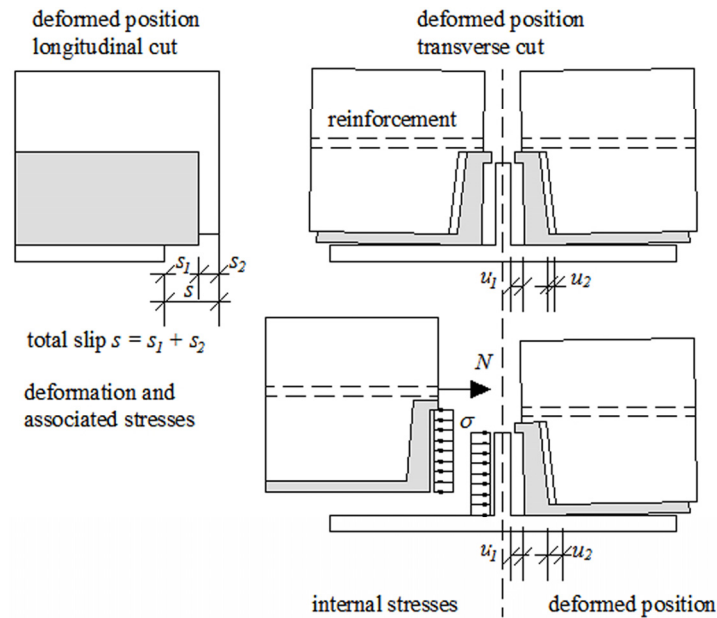
Fig. 23 Mechanical behaviour of the connection

mechanical behaviour of the new connection as illustrated in Fig. 23. This mechanical behaviour is based on several hypotheses presented hereafter. From those, the hypotheses (a) to (g) are based on the work of Thomann and Lebet (2007) and the rest constitute additions of the authors. Those hypotheses are the following:

(a) The total slip s between the slab and the steel girder is the addition of the slip s_1 developed in the embossed steel-cement grout interface and the slip s_2 developed between cement grout and the slab. The same applies to the transversal separation. At each side of the embossed steel plates, the uplift u between the slab and the embossed steel plate is the addition of the uplift u_1 between the embossed steel plate and the cement grout and the uplift u_2 between the cement grout and the slab.

(b) The interfaces that are considered to contribute with their shear resistance are the vertical interfaces: (i) the embossed steel-cement grout interface; and (ii) the cement grout-rough concrete interface. No shear resistance is considered between the cement grout and the upper flange of the steel girder.

(c) The developed normal (confining) stresses in the interface resulting from the equilibrium of forces are considered uniformly distributed on the height of the interfaces.

(d) The two types of interfaces contributing to the resistance are considered to be connected in series, thus the same longitudinal force passes through them.

(e) The slip at each side of the connection is distributed in the two types of interfaces according to the shear stress-slip stiffness defined by the constitutive law of each interface.

(f) The connection shows symmetrical behaviour, meaning that the slip and the uplift (lateral separation) at the two sides of the embossed steel plates are identical.

(g) The cement grout is considered not to be deformed.

(h) No vertical uplift, due to rotation, is considered for the part of the cement grout which

contributes to interfaces' resistance and is situated between the inner rib of the slab and the embossed steel plate, Fig. 23.

(i) The translational movement of the slab is also followed by a rotation resulting to non-uniform transversal uplift, which based on measurements from push-out tests is considered linearly distributed along the interface. However this variation is low enough so that the mean value of the uplift in the middle of the height of the interface can be considered for the calculations.

The translational stiffness of the slab is not constant during the development of slip and the uplift. Initially the slab is not cracked, as it was observed during cyclic loading push-out tests, so initially the translational stiffness is constant. Once the crack is formed and the steel reinforcement is mobilized the stiffness decreases.

The numerical model developed is validated by comparing its prediction with the experimental results of the push-out tests. For the push-out specimens tested the concrete is of type C50/60 and a modulus of elasticity E_{cm} equal to 38600 N/mm^2 is considered according to FIB Model Code
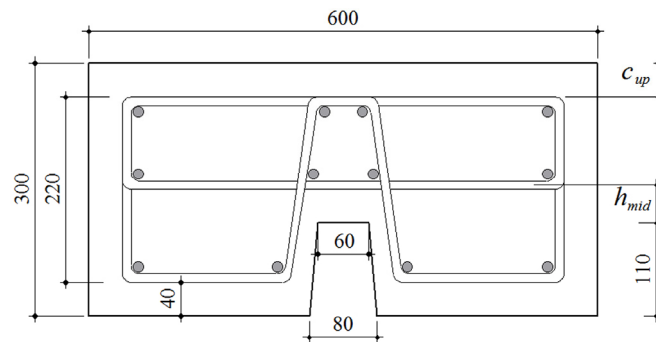

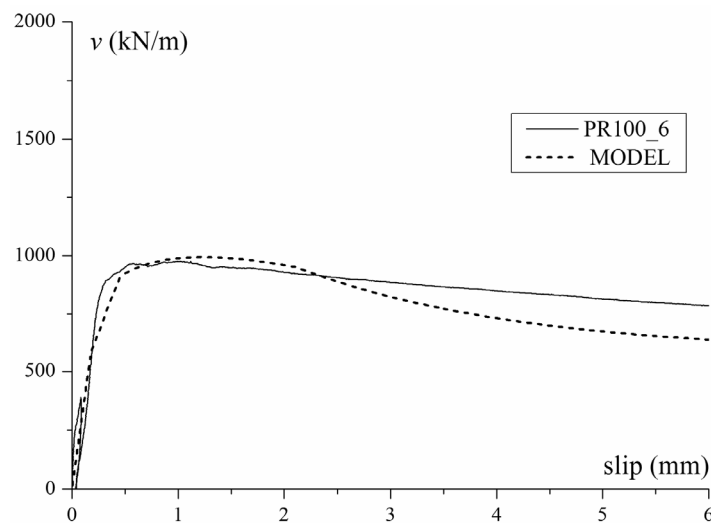Fig. 24 Section of reinforced concrete block used in push-out specimens

Fig. 25 Comparison between numerical model's prediction and push-out test PR100_6
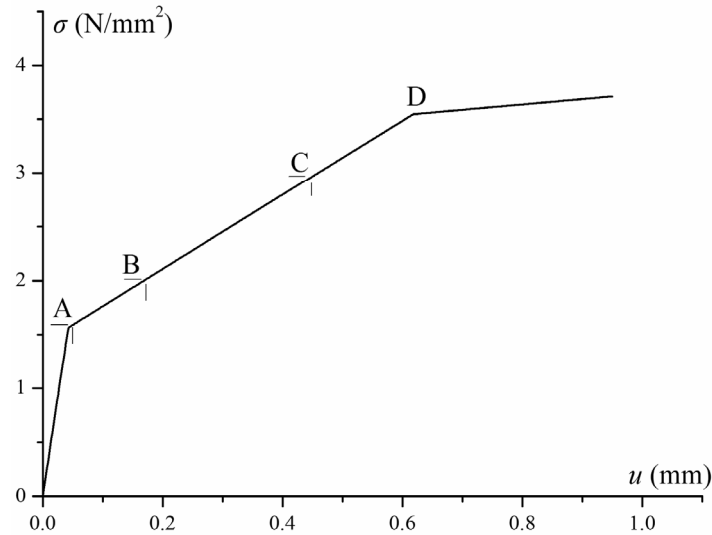
Fig. 26 Normal stress, σ, versus uplift (lateral separation), u, according to the confinement model, (calculated for specimen PR100_6)

2010 (2010). The transversal steel reinforcement has an area of has a diameter of 10 mm spacing 60 mm. The section of typical block of the push-out specimens is illustrated in Fig. 24. The height of the block is 300 mm and the height of the rib equal to 110 mm. As mentioned in the Section 3, the concrete blocks of the tested specimens were submitted to diamond-cutting to check the failure interfaces. Besides failure type, diamond-cutting has revealed that the distance h_{mid} of the centre of the gravity of the middle transversal reinforcement from the edge of the rib was not always the same but varied between 30 mm and 50 mm, resulting consequently to a variation also of the covering of the upper reinforcement. The spacing of the reinforcement for each block of the push-out specimens was also revealed. The variation of the distance h_{mid} and of the reinforcement spacing have an influence in the ultimate resistance and explains the variance of the results of the push-out tests. Thus the model prediction should be validated considering the precise geometric parameters. This is illustrated, for instance for the specimen PR100_6, in Fig. 25. The comparison is satisfactory for slip up to 3 mm. For further slip the model underestimates slightly the connection's performance. This can be attributed to the fact that the real yielding stress of the steel reinforcement can be, as it is often the case in reality, higher than the characteristic yielding stress which was taken into account on the finite element analysis performed for the confinement effect model.

The relationship between the normal stress and the uplift (lateral separation) for this case according to the confinement effect model is presented in Fig. 26. In this figure the first linear branch corresponds to uncracked concrete. After that point the steel rebar is mobilised. The third branch corresponds to yielding of the rebar which is situated just over the concrete rib. It is noted that the finite element analysis, from which the confinement model was developed, simulates the concrete crack propagation due to the uplift, as can be seen in Fig. 13.

The numerical model provides, in addition, the evolution of the secant stiffness of each interface k_i as a function of the total slip s, see Fig. 27, which is especially interesting for defining the end of the elastic behaviour.
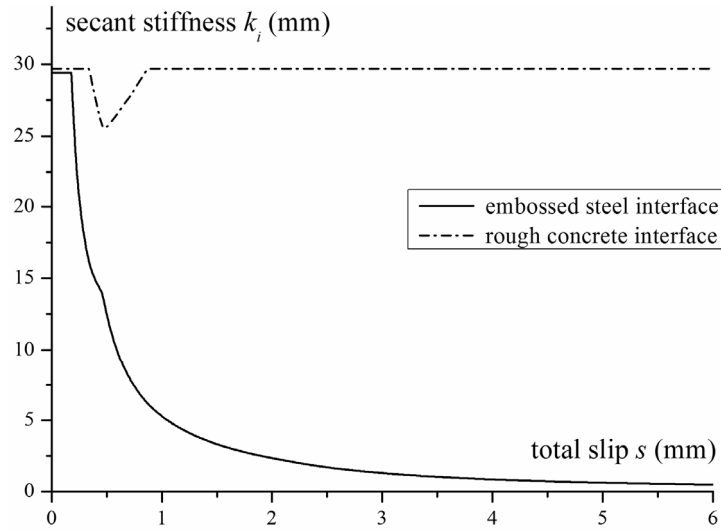
Fig. 27 Prediction of secant stiffness of interfaces (calculated for specimen PR100_6)
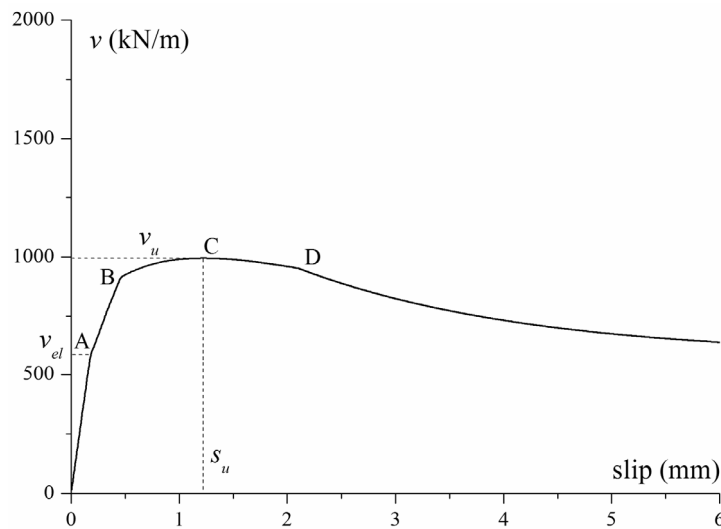

Fig. 28 Characteristic points on model's prediction curve (calculated for specimen PR100_6)

The numerical model's prediction provides some characteristics points A, B, C and D of the structural response of the new connection, see Fig. 28. These points are commentated hereafter:

- Point A (0.175 mm, 569 kN/m) in Fig. 28 corresponds to the end of the elastic behaviour of the connection. Till that point the stiffness of each interface is the elastic stiffness of their constitutive laws, as can be seen in Fig. 27. This point, in Fig. 26, is found to be located slightly after the end of the initial stiff branch of the curve of the confinement stress σ versus the uplift u which concerns the uncracked concrete section. The normal stress, Fig. 26, for this particular example, in point A, has increased to a value of 1.57 N/mm^2. From point A

(end of the elastic behaviour of the interfaces) and after, the stiffness of the embossed steel-cement grout interface decreases, see Fig. 27. The stiffness of the rough concrete-cement grout interface continues for a while to remain constant meaning that this interface continues to exhibit elastic behaviour ($k_2 = k_{el} = 29.7$ N/mm^3). This interface enters the plastic hardening domain of its constitutive law for a total slip between 0.34 mm and 0.9 mm, without however passing to the softening behaviour and finally it enters again the elastic domain for a total slip more than 0.9 mm, see Fig. 27. Point A is of great importance for serviceability limit state, since it defines the end of the elastic behaviour. It will be shown in the Section 4.2 that this point is of great importance also for the fatigue limit state.

- Point B (0.45 mm, 904 kN/m) in Fig. 28 corresponds to the point at which the shear stress at the embossed steel-cement grout interface reaches the ultimate value τ_u, for that particular level of confinement stress $\sigma = 2.01$ N/mm^2, as shown in Fig. 26. After that point the embossed-steel cement grout interface enters the softening behaviour, however the resistance of the connection continues to increase, Fig. 28, since the normal stress also increases, Fig. 26, forcing the softening behaviour of the embossed steel-cement grout interface to be developed at higher values.

- Point C (1.23 mm, 994 kN/m) in Fig. 28 is the first point where the resistance of the connection reaches the ultimate value, V_u, (failure point) and for this particular example the normal stress at this point is equal to 2.97 N/mm^2, Fig. 26. For a limited slip, after that point, the different combinations of the increasing normal stress and the developed shear stress in the embossed steel interface result practically to maintenance of the ultimate resistance, branch CD in Fig. 28.

The decrease of the resistance becomes more abrupt at point D (2.1 mm, 952 kN/m) in Fig. 28, where practically as we see in Fig. 26, point D (3.55 N/mm^2, 0.62 mm), the confinement stress stops to increase significantly. Consequently form that point and after the longitudinal shear force per unit length–slip relationship in Fig. 28 is similar to the softening part of the constitutive law of an embossed steel-cement grout interface with constant normal stress.

4.2 Verification of the connection shear resistance for use in composite bridges

The numerical model provides the ultimate resistance and the whole force-slip response of the new connection. For ultimate limit state the characteristic value of the connection shear resistance is presented in Eq. (5), where v_u is the ultimate shear force per unit length, as predicted by the numerical model and n_v is a reduction factor equal to 0.89 which was found by using in the numerical model, the 5% fractile values for the failure criteria of the interfaces (Papastergiou 2012).

$$v_{Rk} = v_u \cdot n_v \tag{5}$$

The verification at ultimate limit state is performed by Eq. (6), taking into account a partial factor γ_v equal to 1.25 for steel-concrete composite connections (SIA 264 2003). The design value of the longitudinal shear actions is expressed by the term v_{Ed} and is due to forces acting in the connection after curing of the cement grout.

$$v_{Ed} \cdot \gamma_v \leq v_{Rk} \tag{6}$$

Concerning the fatigue limit state, the experimental investigation has shown that the connection

is resistant to repeated loading for a ratio of the maximum cyclic shear load versus the ultimate resistance V_{max}/V_u ranging between 0.41 to 0.55. The numerical model provides, as presented in Fig. 28, the point A which is the end of the elastic behaviour. Up to this point the stiffness of the interfaces remains constant (elastic stiffness). In other words the shear stresses in the interfaces remain elastic regardless of the increase of the normal stress, since it was found that the elastic stiffness is independent of the normal stress (Papastergiou and Lebet 2011). For repeated loading with shear stresses remaining elastic the behaviour of stabilization of the residual slip is guaranteed allowing for use of Eq. (4). For the specific case of the model prediction for push-out specimen PR100_6, Fig. 28, the application of Eq. (4), with $s_{V max,I}$ equal to the slip at the end of the elastic response, results in a number of cycles to failure in order of several billions, Eq. (7).

$$N_f = \left(\frac{s_u}{s_{V max,1}} \right)^{1/b_{con}} = \left(\frac{1.23}{0.175} \right)^{1/0.072} \approx 578 \text{ billion cycles} \tag{7}$$

This is the case also for other connection geometry as was found by parametric analysis (Papastergiou 2012) in which the connection geometry was varying according to typical cross sections of practise. Concluding, since the number of cycles to failure is far higher than the service life of the bridge, the longitudinal shear resistance, v_{el}, at the end of the elastic behaviour of the connection as obtained from the numerical model for static loading, Fig. 28, can be used as a fatigue limit.

Finally the verification of the connection shear resistance with respect to the fatigue limit is expressed by Eq. (8).

$$v_{Rk,fat} = v_{el} \cdot n_{v,el} \geq v_{long} + \gamma_{fat} \cdot \Delta v(Q_{fat}) \leq 800 \text{ kN/m} \tag{8}$$

$v_{Rk,fat}$: characteristic value of the shear connection resistance for fatigue limit state

v_{el} : longitudinal shear force per unit length, at the end of the elastic behaviour of the connection's structural response (fatigue limit)

v_{long} : the design longitudinal shear force per unit length due to permanent loads acting in the connection after the realization of the connection, (v_{long} includes a partial factor γ_v)

γ_v : partial factor of the connection resistance equal to 1.25 (SIA 264 2003)

$n_{v,el}$: conversion factor for the connection longitudinal shear resistance at limit of fatigue, equal to 0.74, found in the same way as for the conversion factor n_v mentioned above

γ_{fat} : partial factor for fatigue strength equal to 1.15 (SIA 264 2003)

$\Delta v(Q_{fat})$: variation of the longitudinal shear force per unit length due to the selected fatigue model load

In Eq. (8) the value of 800 kN/m represents a maximum for a connection for typical twin-I girder steel-concrete composite bridges found in Switzerland when the model of Meystre and Lebet (2011) is used for $\Delta v(Q_{fat})$.

5. Conclusions

This paper presents the experimental investigation on a new type of connection for steel-concrete composite bridges and the numerical model developed to predict the connection behaviour. Important conclusions are drawn from the performed work:

(1) The connection's behaviour both in static and cyclic loading results from the resistance of the interfaces that constitute the connection.
(2) An important factor is the confinement effect on the interfaces. The confinement effect is the increase of the normal stress applied on the interfaces due to the interaction of the kinematic law and the translational stiffness of the slab that encloses the connection. The confinement effect is responsible for extending the constitutive and kinematic laws to a higher level of normal stress. It defines the shear stress path of the developed shear stresses in the interfaces and determinates together with the behaviour laws of the interfaces the connection's resistance and deformation capacity.
(3) Damage due to cyclic loading of the connection is expressed by the development of a residual slip which increases with a number of cycles. This increase is stabilized as long as the stresses in the interfaces remain elastic.
(4) A safe fatigue failure criterion is proposed for the connection which says that as long as the accumulated slip under maximum cyclic shear load, $s_{V\max,N}$, does not exceed the failure slip for static loading, s_u, failure due to cyclic loading does not occur and the remaining capacity is equal to that obtained for static loading.

The numerical model developed simulates the force-slip relationship of the connection for static loading providing the ultimate shear resistance and the fatigue limit as well.

Acknowledgments

References

ABAQUS (2011), *Software Package*, Simulia, Version 6.11-2.
Centre Suisse de la Construction Métallique (2005), C5/05 steelwork, *Tables de construction*, Switzerland. [In French]
Eurocode 1, European Standard (2003), *Actions on Structures – Part 2*: *Traffic Loads on Bridges*, EN 1991-2.
Eurocode 2, European Standard (2004), *Design of Concrete Structures – Part 1-1*: *General Rules and Rules for Buildings*, EN 1992-1-1.
Feldmann, M., Hechler, O., Hegger, J. and Rausher, S. (2008), "Fatigue behavior of shear connectors in high performance concrete", *Proceedings of the 2008 Composite Construction and in Steel and Concrete Conference VI*, Devil's Thumb Ranch, Tabernash, CO, USA, July.
FIB (2010), *Model Code 2010*
HMB (2000), *Inductive Displacement Transducers*, Technical brochure.
Kim, H.Y. and Jeong, Y.J. (2010), "Ultimate strength of a steel–concrete composite bridge deck slab with profiled sheeting", *Eng. Str.*, **32**(2), 534-546.
Meystre, T. and Lebet, J-P. (2011), "*Modèle de charge de trafic actualisé pour les dalles de roulement en*

béton", Provisory Report, OFROU-AGB 2009/005. [In French]

Oh, B.H. and Kim, S.H. (2007), "Realistic models for local bond stress-slip of reinforced concrete under repeated loading", *ASCE Struct. Eng. J.*, **133**(2), 224-216.

Papastergiou, D. (2012), "Connections by adhesion, interlocking and friction for steel-concrete composite bridges under static and cyclic loading", EPFL Thesis, No. 3501, Lausanne, Switzerland.

Papastergiou, D. and Lebet, J.P. (2011), "New steel-concrete connection for prefabricated composite bridges", *Stahlbau*, **80**(12), 894-903.

Papastergiou, D. and Lebet, J.P. (2014), "Experimental investigation and modelling of the structural behaviour of confined grouted interfaces for a new steel-concrete connection", *Eng. Struct.*, **74**, 180-192.

Rauscher, S. and Hegger, J. (2008), "Modern composite structures made of high performance materials", *Proceedings of the 2008 Composite Construction and in Steel and Concrete Conference VI*, Devil's Thumb Ranch, Tabernash, CO, USA, July.

SIA 261 (2003), Registered code of the swiss standards association, *Actions on Structures*, SN 505 261.

SIA 264 (2003), Registered code of the swiss standards association, *Composite Steel and Concrete Structures*, SN 505 264.

Thomann, M. and Lebet, J.P. (2007), "Design method for connections by adherence for steel-concrete composite bridges", *Struct. Eng. Inter.*, **17**(1), 86-93.

VSL (2002), *Grouting of Post-Tensioning Tendons*, VSL Series No.5.

CC